Solute Diffusion of Hydrogen Isotopes in Tungsten - a gas loading experiment

G. Holzner[1], T. Schwarz-Selinger[1], T. Dürbeck[1] and U. von Toussaint[1]

[1]Max-Planck-Institut für Plasmaphysik, Boltzmannstr. 2, D-85748 Garching, Germany

E-mail: georg.holzner@ipp.mpg.de

Abstract. The diffusion of protium and deuterium in tungsten is measured in gas loading experiments as a function of temperature for a hydrogen isotope loading pressure of 500 mbar and temperatures between 1600 K and 2600 K. The diffusion parameters are measured from degassing rates of both a single and a poly crystalline tungsten cylinder by mass spectrometry. The data is analysed assuming an Arrhenius-like temperature dependence of the diffusivity and following the classical analysis approach of Frauenfelder [1]. For deuterium in tungsten an activation energy of $E_A^D = 0.28 \pm 0.06$ eV is obtained. For protium the activation energy is identical within the uncertainty limits.

PACS numbers: 52.40.Hf, 66.30.J-, 89.30.Jj

Submitted to: *Phys. Scr. / PFMC-17*

1. Introduction

For the design of future fusion devices the transport and retention of hydrogen is of particular importance. Diffusion and trapping of radioactive tritium through plasma-facing materials can result in intolerable in-vessel inventories and undesired losses to the coolant. Similarly an enhanced near-surface inventory may affect plasma operation due to uncontrolled mobilization of these inventories during transients. These effects can to some extend be modelled using diffusion-trapping codes such as TMAP7 [2], TESSIM [3] or MHIMS [4]. Crucial for reliable code-based predictions is the precise knowledge of key parameters entering the simulation, notably – besides the defect densities – the diffusion and solubility constants. The huge scatter and inconsistent trends of the available data for the latter quantities led to the recommendation by Causey [5] that the data of Frauenfelder [1] is presumably the most reliable one – with the consequence that since then the modelling results within the fusion community are almost exclusively based on Frauenfelder's values for protium in tungsten. However, it needs to be kept in mind that Frauenfelder's experiments in the 1960's had to rely on the measurement and analysis technique of that period and that his specimen was technical grade tungsten which necessitated an extensive discussion of the potential influence of defects and impurities on the results. In the last decade several papers with

density functional calculations of the activation energy appeared [6],[7],[8] which also showed considerable scatter in the results (0.21 eV, 0.25 eV, 0.38 eV, respectively); also discussions are ongoing in which temperature region the solute diffusion regime is valid [9].

Given the importance of these basic quantities, a new device was designed with the purpose of measuring solubility and diffusion of protium and deuterium in tungsten using poly and single crystalline cylindrical samples. First time-resolved thermal desorption spectroscopy (TDS) measurements have been performed. Heating-rates are varied between 15 K/s and 20 K/s for the outgassing of the specimen. The probability distribution of the relevant parameters have been derived by fitting the long-term decay of the hydrogen effusion - which is the same approach that Frauenfelder used for his experiments. The loading temperatures are varied between 1600 K and 2200 K at 500 mbar protium or deuterium pressure. The degassing temperatures are varied between 1600 K and 2600 K.

In the following the term hydrogen refers generically to all three hydrogen isotopes. Otherwise the isotope of interest is directly addressed as either protium (H), deuterium (D) or tritium (T).

2. The Experimental Setup

The experimental setup is schematically shown in figure 1. Its basic design is very close to the one of the original set-up of Frauenfelder [1]. The tungsten specimen is placed in a double-walled quartz-glass tube. This enables an efficient water cooling of the glass tube to cool the inner wall which is exposed to the thermal radiation of the specimen when heated. Hereby an excessive outgassing of hydrogen as well as hydrogen permeation through the inner wall of the glass tube is suppressed while the specimen is degassed in the measurement phase. Two tungsten specimens are investigated and compared with identical loading and degassing conditions: one poly crystal and one single crystal. This allows to investigate the influence of the presumably lower defect density in the single crystal and allows also to scrutinize the assumption that the defect density in a poly crystal is negligible at outgassing temperatures higher than roughly 1400 K. Each of the cylindrical specimens has the same geometry, a diameter of 15 mm and a length of 48 mm. The poly crystal was delivered from Louis Renner GmbH, it was sintered at over 3000 °C under hydrogen atmosphere, its nominal density was given to be around 19.2 $\frac{g}{cm^3}$. The tungsten single crystal was delivered by MaTecK GmbH, the manufacturer states that the single crystal has a 110 orientation with an accuracy better than 2°, concerning impurities the manufacturer states the amounts of foreign elements as follows: C $<$ 3 ppm, H $<$ 1 ppm, O = 9 ppm, N $<$ 5 ppm, Cu = 1.6 ppm, Fe = 1.8 ppm, Ni $<$ 1 ppm, Pb = 0.3 ppm, Si = 0.3 ppm and Ga, Hf and Ta are below the detection limit. It came unpolished and was turned down to a diameter of 15 mm. The specimen is mounted in the middle of the glass tube by a dove-tail connection to a tungsten shaft with diameter of 5 mm. The minimal load bearing diameter of the tungsten shaft directly at the mounting area is 3.5 mm. The tungsten shaft itself sits in a stainless steel flange that is mounted on a glass-steel flange on top of the glass tube. A copper water-cooled inductive coil with an inner diameter of 50 mm is placed around the glass tube and is used for contactless heating of the specimen. The

inductive furnace TruHeat MF 5040 was purchased from Trumpf Hüttinger GmbH and has a nominal peak power of 40 kW, the frequency is autonomously adjusted between 20 - 100 kHz. The furnace is operated with a temperature controller. For temperature measurement and control a type-C thermocouple is directly welded to the specimen by laser welding. A second temperature measurement is implemented by using a single wavelength pyrometer at direct line of sight from underneath through a quartz glass window, type VPCF40UVQ-L-316L from Vacom. The pyrometer uses the wavelength of $\lambda = 1.27\,\mu$m where the emissivity of tungsten

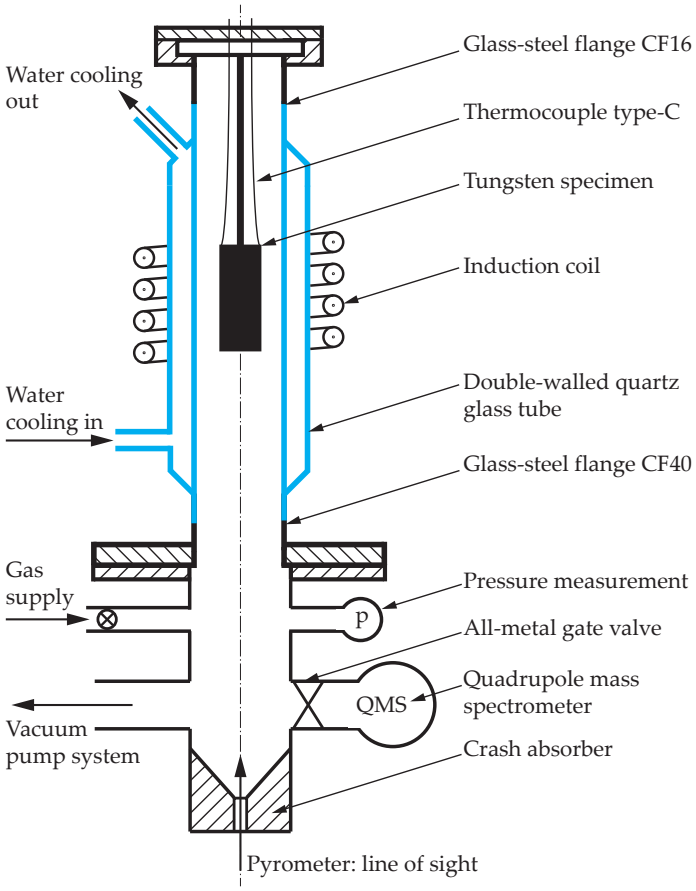

Figure 1: Experimental arrangement that is used for the loading and degassing of the tungsten specimen. Parts which are actively water-cooled are indicated in blue.

does not change with temperature [10]. The emissivity of the tungsten specimen and the reflection and absorption of the quartz glass window is adjusted by calibrating the feedback temperature of the pyrometer against the temperature measurement of the thermocouple. The pyrometer is necessary only when the temperature of the specimen exceeds 2573 K (2300 °C) where the calibrated temperature measurement range of the type-C thermocouple ends. The accuracy for the temperature measurement is estimated to ± 13 K at 1600 K and +23 K and -37 K at 2600 K. At the lower temperatures only the accuracy of the type-C thermocouple wires of $\pm$ 1 % is considered. Temperature readings of type-C thermocouple and pyrometer are consistent. At high temperatures for 3 - 5 min a slow temperature drift of the pyrometer temperature reading towards lower temperatures is observed and leads to

an additional uncertainty. This is consistent with a decrease of injected power from the inductive furnace and leads to an increased temperature uncertainty at high temperatures. For example for an outgassing temperature of 2400 K a total drift of 14 K is observed. The inductive coil fully covers the specimen which heats the specimen over the whole length. Within the acccuray of a disappearing filament pyrometer no temperature variation along the tungsten cylinder (ie. convective cooling by hydrogen) could be detected. We thus assume that the specimen exhibits no temperature variation along the z-axis during the loading phase. Two pressure measurement devices are used, a Pfeiffer capacitance gauge that can measure pressures between 1 and 1100 mbar and a Pfeiffer cold cathode full range gauge which can measure pressures between $5 \cdot 10^{-9}$ and 1 mbar. The gas loading vessel is attached to the TESS vacuum vessel [11] which contains the quadrupole mass spectrometre (QMS) DMM 422 from Inficon Liechtenstein. The QMS chamber is pumped via two turbo pumps in series which enhances the compression ratio and such the pumping speed is considered to be independent of pressure in the vessel in the pressure range of interest.

3. Measurement Procedure

For the measurement phase when the outgassing of the specimen is measured with the QMS the turbo pump at the vacuum system of the gas loading vessel is disconnected. To purify the hydrogen that is used for loading the hydrogen pipe is led through a cold trap, a vessel filled with liquid nitrogen (77 K). The measurement procedure principally consists of loading and degassing of the specimen. Figure 2 shows a typical loading and degassing cycle. The upper graph shows the temperature of the specimen, the graph also includes the degassing from the specimen in the degassing phase. The lower graph shows the temperature gradient. Initially the vessel was evacuated down to at least $5 \cdot 10^{-8}$ mbar. Then the pumping is stopped, the turbo pump is disconnected from the loading vessel and the vessel is filled with gas. At phase 1 the vessel is filled to 500 mbar hydrogen pressure and the temperature of the specimen is at room temperature - this is the beginning of the gas loading. Then the temperature is ramped up to the desired loading temperature, in this case 2000 K, and held constant. The specimen is held at this temperature until thermal equilibrium (i.e. a constant concentration of dissolved hydrogen) for this temperature is reached (phase 2), in this case a holding time of 30 min at 2000 K is chosen. The necessary holding time has been derived by a sequence of increasingly longer loading times, until the measured retained amount of hydrogen saturated. After that the specimen is cooled down by switching off the heating. The cool down rate from 2000 K is initially about 35 K/s. Later the cooling is no longer radiation but gas cooling/convection dominated and the cool down rates become smaller. The cool down rate is sufficiently fast to trap a significant amount of the hydrogen initially present in the sample. Nevertheless some of the dissolved hydrogen is able to escape the specimen during quenching which results in a decay of hydrogen concentration to a lower level than the one previously reached at equilibrium for the loading temperature. This undesired outgassing cannot be measured because the QMS in the neighbouring TESS-chamber can only be run up to a pressure of about $5 \cdot 10^{-6}$ mbar. When the specimen has reached 373 K (100 °C) the vessel is pumped

to about $1 \cdot 10^{-7}$ mbar, the start of the pumping is marked as phase 3. The pumping takes about 15 minutes. Then the valve to the QMS chamber is opened at phase 4, the beginning of the degassing phase. The QMS signal (counts per second) is converted to an atom flux by using a calibrated gas leak bottle at the end of every measurement. The flux of deuterium atoms is given as red signal at the right vertical axis. The degassing phase starts when the temperature is ramped up again to a constant temperature and the hydrogen in the specimen is mobilised. After the temperature has reached a constant level the deuterium atoms flux decays as a consequence of the reduction of the hydrogen concentration gradient at the surface. At the end, shortly after 5000 s a dip with a subsequent rise before the overall signal decay is observed after the heating is switched off - this dip can be seen after every measurement. As reason we suspect temporarily increased wall pumping: after the oven is switched off the temperature of the inner glass wall decays rapidly due to the strong reduction of radiation heating.

This whole procedure is repeated for two ramping rates, loading temperatures between 1600 K and 2200 K and different outgassing temperatures between 1600 K and 2600 K.

4. Sample preparation

Before the start of the measurement campaigns, each of which consist of several loading-degassing cycles, each specimen is high temperature treated at 2600 K iteratively for a total of 10 h in hydrogen and 10 h in vacuum. This causes massive grain coarsening and annealing of lattice defects because of the extended holding time at this high temperature. It also results in quasi-static lattice conditions for the following measurements at temperatures $\leqslant$ 2600 K. The long holding at high temperature in hydrogen will also cause at least partial removal of impurities from the specimens. Common tungsten impurities like oxygen can diffuse to the surface, react with the hydrogen being present and desorb. The whole preparation process was started in hydrogen atmosphere rather than in vacuum to hinder the formation of tungsten-carbides on the surface of the specimen because those would be hard to get rid off even in hydrogen atmosphere and high temperatures. The specimen afterwards undergoes the loading/degassing cycles for the measurements.

5. Modelling

5.1. Diffusion

Our modelling of H/D-diffusion in tungsten is based on the diffusion equation in 3-D cylindrical geometry under the assumptions of an initially constant hydrogen isotope concentration in the cylinder after gas loading when the hydrogen concentration in the specimen reached equilibrium before the cool-down phase (phase 2 at almost 2000 s in figure 2). We assume diffusion limited outgassing [5] i.e. that the surface concentration is zero throughout the hydrogen release, thus yielding Dirichlet boundary conditions. In full generality a coupled system of equations for the temperature field in the cylinder $T(\vec{r},t)$ and

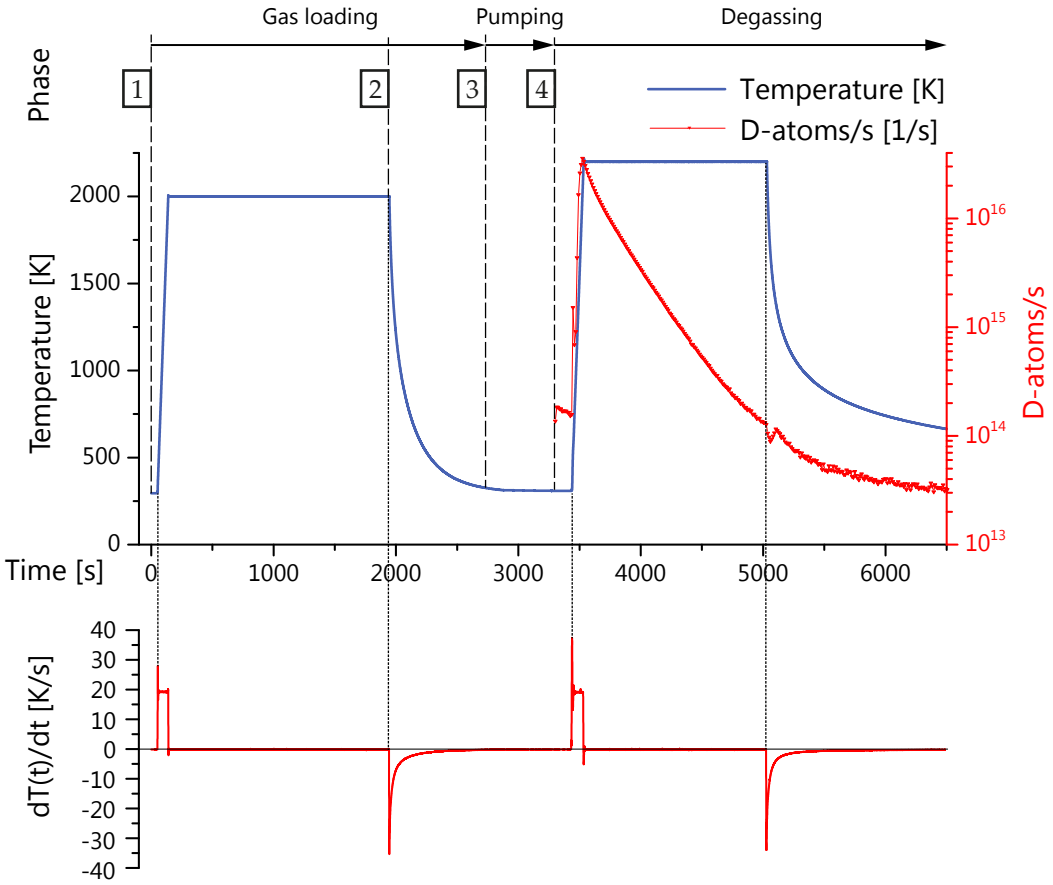

Figure 2: Schematic measurement procedure: gas loading of the specimen at constant temperature of 2000 K and constant pressure of 500 mbar (phase 1 and 2). After loading the vessel is pumped (phase 3) and the valve to the QMS chamber is opened to measure the degassing of the specimen (phase 4). In the lower panel the temperature gradient of the specimen is displayed.

the concentration profile $c\left(\vec{r}, D\left(T\left(\vec{r},t\right)\right),t\right)$ needs to be solved, since the diffusion depends on temperature. However, due to the high thermal conductivity of tungsten (increasing from 126 W/(K·m) above 2300 K [12] to 174 W/(K·m) [13] at room temperature) and the moderate upper limit of the cooling rates of the cylinder (at most 35 K/s, see fig. 2) the temperature profile in the cylinder is almost flat. Also the reduction of the thermal conductivity by the applied magnetic field is negligible at temperatures above room temperature [13]. The largest temperature differences in a loading-degassing cycle between the peak temperature in the core of the cylinder and at the outer radius are of $O\left(1\mathrm{K}\right)$ for a cylinder loaded at 2000 K. In the following we thus use a time dependent but spatially constant temperature profile $T = T\left(t\right)$, where the time dependent temperature values are taken from thermocouple measurements.

The cylindrical coordinate system allows to express the time-dependent concentration $c\left(r,z\right)$ of hydrogen in a cylinder with radius $a\left(r : 0 \leq r < a\right)$ and length $2L\left(z : -L < z < L\right)$

as product of one-dimensional functions in each coordinate (see eg. [14], chapter 8.4, Eq.5)

$$c(r,z \mid t,a,L) = c_0 \psi(z \mid t,L)\, \chi(r \mid t,a) \tag{1}$$

where $\psi(z)$ expresses the hydrogen concentration along the cylinder axis, whereas $\chi(r)$ expresses it in radial direction.

For diffusion limited boundary conditions $\psi(z)$ and $\chi(r)$ are given by

$$\psi(z \mid t,L) = \frac{4}{\pi} \sum_{n=0}^{\infty} \frac{(-1)^n}{(2n+1)} \exp\left[-(2n+1)^2 \frac{\pi^2}{4L^2} D(T)\, t\right] \cos\left(\frac{(2n+1)\pi z}{2L}\right) \tag{2}$$

and

$$\chi(r \mid t,a) = \frac{2}{a} \sum_{m=1}^{\infty} \exp\left[-\alpha_m^2 D(T)\, t\right] \frac{J_0(r\alpha_m)}{\alpha_m J_1(a\alpha_m)}. \tag{3}$$

In the two previous equations $D(T)$ denotes the hydrogen isotope diffusion and $J_0(x)$ is the Bessel function of order zero of the first kind. Similarly $J_1(x)$ is the Bessel function of the first kind of order one. The parameters α_m are the consecutive positive roots of $J_0(\alpha a_m) = 0$, ie. $\alpha_1 = (\xi_1/a), \alpha_2 = (\xi_2/a), \ldots$ with $\xi_1 \approx 2.4048$, $\xi_2 \approx 5.5201, \ldots$.

The expression can be simplified by using the recurrence property of the Bessel functions

$$\int_0^a \mathrm{d}r\, r^{n+1} J_n(\beta r) = \frac{1}{\beta} a^{n+1} J_{n+1}(a\beta), \; n > -1 \tag{4}$$

to average over the radius to get

$$\langle \chi(r \mid t,a) \rangle = \frac{1}{\pi a^2} \int_0^a \mathrm{d}r\, 2\pi r\, \chi(r \mid t,a) = \frac{4}{a^2} \sum_{m=1}^{\infty} \frac{1}{\alpha_m^2} \exp\left(-\alpha_m^2 D(T)\, t\right). \tag{5}$$

The total amount of hydrogen as function of time for constant temperature can be calculated using equation 5 in equation 1, followed by integration over the cylinder length

$$\begin{aligned} \mathrm{M}(t) =& c_0 \int_{-L}^{L} \mathrm{d}z\, \pi a^2 \langle \chi(r \mid t,a) \rangle\, \psi(z \mid t,L) \\ =& c_0 \frac{64\mathrm{L}}{\pi} \left(\sum_{m=1}^{\infty} \frac{1}{\alpha_m^2} \exp\left(-\alpha_m^2 D(T)\, t\right) \right) \left(\sum_{n=0}^{\infty} \frac{1}{(2n+1)} \exp\left[-(2n+1)^2 \frac{\pi^2}{4L^2} D(T)\, t\right] \right). \end{aligned} \tag{6}$$

In the limit of long times $\left(t > a^2/(100 \cdot D(T))\right)$ and for the present dimensions of the specimen (cylinder diameter significantly smaller than the length) the first term in equation 6 dominates the decay of $\mathrm{M}(t)$. During the outgassing the radial concentration profile turns from a concentration profile with higher order contributions of the Bessel functions ($m > 1$) i.e. with sharp features at the sample boundaries into a smooth concentration profile (with only the $m = 1$ term - the fundamental mode - being relevant). The outgassing features of the specimen in experiment support this assumption, i.e. displaying an exponential decay of the degassing signal for longer times at constant temperature (when the "peak" at the beginning of the degassing signal has vanished, see e.g. figure 5 at about t=2700 s).

The leading outgassing term (ie. the time derivative of Eq. 6) for long times and constant temperature is thus given by

$$\dot{M}(t) \propto \exp(-\gamma t) \propto c_0 \exp\left(-\alpha_1^2 D(T)\, t\right) = c_0 \exp\left(-4\xi_1^2 D(T)\, t/d^2\right), \tag{7}$$

where the last expression has been written such that it connects with the equation used by Frauenfelder (cf. [1], Eq. 4). For the subsequent analysis an Arrhenius-like dependency of the diffusion constant on the temperature is assumed

$$D(T) = D_0 \exp(-E_A/kT), \tag{8}$$

with activation energy E_A for the diffusion and a pre-factor D_0.

For the numerical modeling the previous equations are discretised in time to take into account the varying temperature. The time-step is chosen such that the temperature change within 1 time-step is always smaller than 0.01 Kelvin and otherwise a time-step of 1 s is used. Tests with even smaller time-steps did not show any impact on the results.

5.2. Cooling cycle

The modeling approach presented in the previous section has been used to assess the loss of hydrogen from the cylinder during the cool-down phase until the start of the outgassing cycle. After sufficiently long loading time (which depends on the loading temperature and ranges from 180 min at 1600 K to 25 min at 2200 K for 500 mbar hydrogen pressure) the initial concentration profile is almost constant throughout the cylinder and can be assumed to be in thermodynamic equilibrium, i.e. the concentration of dissolved hydrogen is a function of the sample temperature and hydrogen gas pressure only. The moment the heating is stopped the cylinder cools down. Initially the heat loss is dominated by radiation losses, at later stages by convective losses to the surrounding hydrogen gas. In Fig. 3 the time traces of the cylinder temperature and the corresponding retained amount of hydrogen (normalised to the initial amount) are displayed for three different diffusion activation energies. Initially the hydrogen loss is fast due to the high diffusivity at temperatures well above 750 K and the hydrogen depletion dominantly from the outer parts of the cylinder. At later times the hydrogen loss is significantly lower because close to the cylinder surfaces the hydrogen concentration is almost zero, hence here also the gradient of hydrogen concentration is very small. In addition the hydrogen transport is slowed down by the decreasing temperature and becomes negligible below 450 K . Nevertheless, the cylinder looses around 35% of its initial amount of deuterium for an activation energy of 0.30 eV and a pre-factor of 0.0016 cm^2/s. Experiments show that the loss from the specimen at room temperature is not measurable within the uncertainty limits for equally executed experiments where only the dwell time (i.e. pumping time) after loading was varied from about 15 min to one week. Also the hydrogen concentration becomes non-uniform during the cooling. The normalised initial hydrogen concentration profile of the cylinder as well as the profiles immediately before the degassing-sequence (t= 1500 s) along the radial and vertical directions are given in Fig. 4. For comparison also the fundamental $m = 1$-profile is given as dotted line. From the difference in the shapes the presence of higher order terms ($m > 1$) at the onset of the degassing-sequence can be concluded.

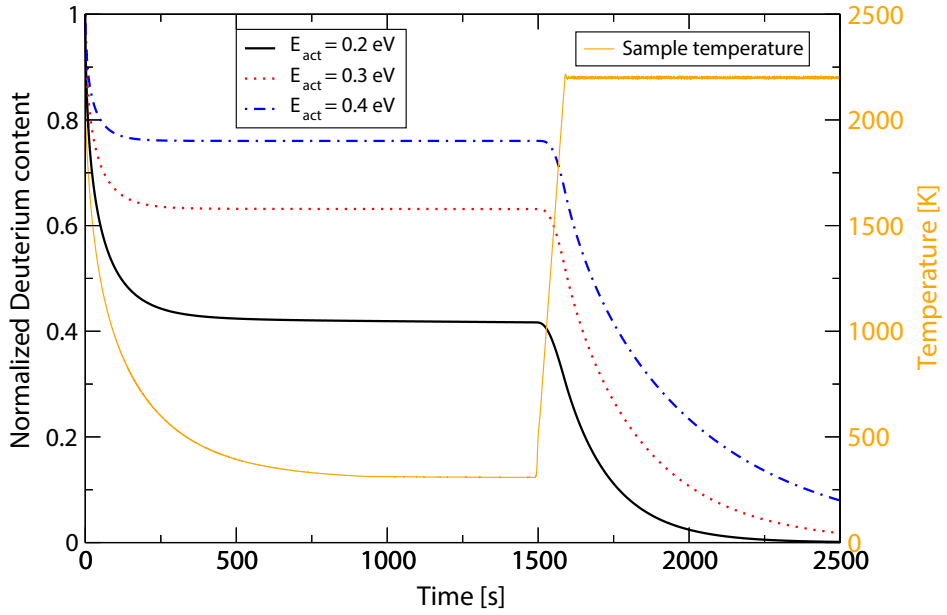

Figure 3: The amount of deuterium retained in the tungsten cylinder (dimensions: diameter: 15 mm; length: 48 mm) calculated as function of time for three different diffusion activation energies of 0.2 eV, 0.3 eV and 0.4 eV and a common pre-factor of 0.0016 cm^2/s. The amounts of deuterium are all normalised to the initial amount. The loading temperature has been 2200 K. The measured sample temperature during the cool-down (here for a deuterium pressure of 500 mbar) is also indicated (scale is given on the right hand-side). The largest loss during the cooling of the sample in hydrogen atmosphere occurs immediately after switching off the heating. The retained amounts after the sample has reached room temperature are roughly 78%, 65% and 45% for assumed diffusion activation energies of 0.4 eV, 0.3 eV and 0.2 eV, respectively.

5.3. Influence of Traps

Trap sites, i.e. lattice positions with a higher activation energy for detrapping compared to the regular interstitial diffusion may affect the observed diffusion properties. These trap sites in the tungsten lattice may be given by vacancies or by impurity atoms like carbon. At present we consider the influence of traps in the sample volume on the outgassing behaviour for both the single and poly crystalline sample as negligible for the following reasons:

- Due to the high defect formation energy in tungsten of 3.67 ± 0.2 eV [15] for monovacancy formation the intrinsic equilibrium defect density is extremely low even at temperatures of 2400 K.
- The impurity concentration in single crystalline tungsten and sintered poly crystalline tungsten is minimal and should be reduced even further during the extended periods the sample is kept at high temperatures in hydrogen atmosphere.
- Traps with a large activation energy (e.g. $E_{act} \geq 1.4$ eV) would be filled during the loading stage. These traps would remain partially filled during the cooling phase and

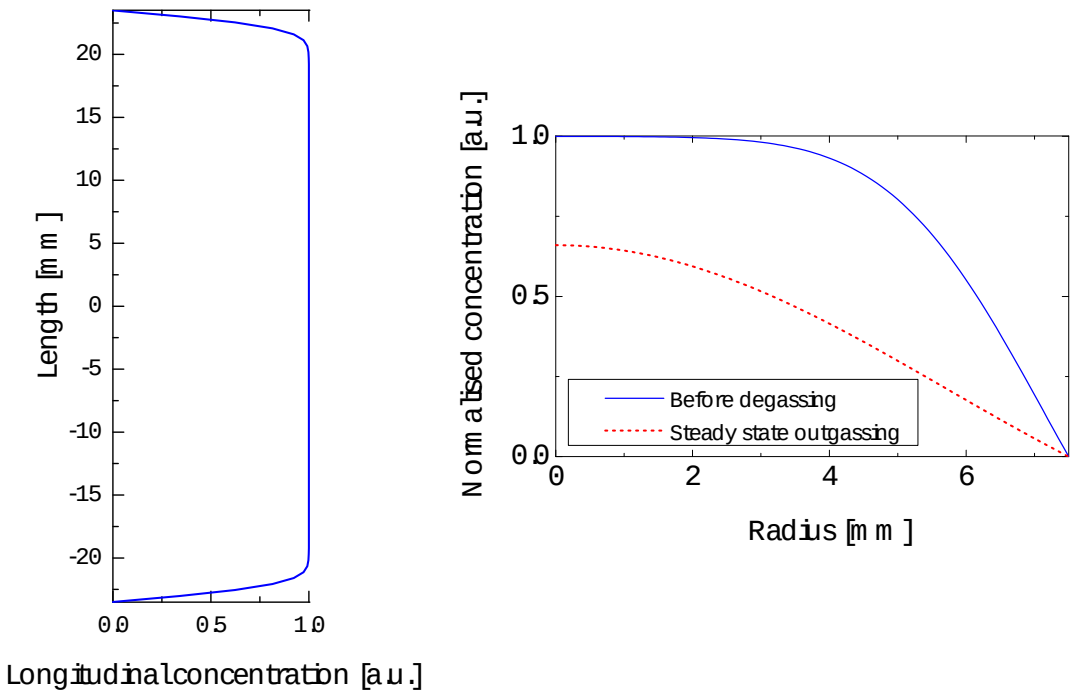

Figure 4: Left panel: Longitudinal concentration profile of the specimen after loading and cool down. The radial concentration is shown in the right-hand side panel where the solid line shows the concentration profile after cool down and before the outgassing. The dotted line exemplarily shows the hydrogen concentration profile at steady state outgassing conditions in the sample when the temperature already has reached the constant plateau. The concentration profile during the outgassing proceeds from the non-sinusoidal profile (i.e. higher harmonics in the Bessel function, $m > 1$, see equation 8) before outgassing towards a smooth profile where the fundamental mode dominates - this can also be seen in the degassing signal when the "peak" decays towards a single-exponential decay (visible as linear decay in the log-plot).

would cause as a characteristic signature in a subsequent TDS measurement. This has not been observed in control experiments.

Although we have no indication of an influence of traps in the sample volume we observe a non-monotonic behaviour of the hydrogen signal at the beginning of the heating ramps (i.e. a "spike", to be seen at the begin of the heating ramp in figure 5 at $t \approx 2200$ s). The magnitude of this feature depends on the time between the loading phase and the onset of the outgassing cycle. We attribute that to the formation of a thin tungsten-oxide layer on the cylinder surface which can influence the hydrogen release. Since tungsten oxide layers evaporate rapidly above 1570 K [16] there is no effect on the slope data used for the present estimation of the diffusion constant. It could, however, affect the estimation of the solubility parameters in some circumstances, i.e. if the oxide layer forms already during the cool-down phase and may also influence the joint (full model based) estimation of solubility and diffusion

parameters (c.f. section 5.4).

5.4. Solubility

As outlined in the previous subsection determination of the solubility of hydrogen in tungsten faces some challenges. At the end of the loading phase the cylinder is assumed to be in thermodynamic equilibrium. Again relying on an Arrhenius-like description the solubility is given by

$$S(T,p) = S_0 \exp(-E_S/kT) \tag{9}$$

with E_S being the heat of solution. However, in the moment when the induction furnace is switched off the cylinder cools down and the sample starts to loose hydrogen. Unfortunately the lost amounts for the different loading temperatures are unknown because this depends on the yet unknown temperature dependent diffusion and cannot be measured because of the loading gas still present in the glass tube. This implies that a self-consistent model has to determine all 4 unknown parameters simultaneously (E_{act}, D_0, E_S and S_0) by the joint evaluation of several loading-degassing measurements. The initial results of that approach (which - for brevity - is omitted here and will be presented in a forthcoming paper) are in reasonable agreement with the solubility data provided in [1] but the possible influence of intermittent surface oxide layers needs to be scrutinized, ie. by using differently sized specimen.

6. Results

Figure 5 exemplarily shows the outgassing of a single and a poly crystalline sample that are loaded equally at 500 mbar deuterium at 2000 K and outgassed at 2000 K with a 20 K/s ramp. Displayed is the logarithm of the quadrupole mass spectrometer signal for mass channel m = 4 (ie. molecular deuterium D_2), taking into account the previously derived calibration factor for deuterium. The signal rises until a constant temperature of 2000 K is reached at about 2250 s, then both signals decay. After a non-exponential decay at the beginning both signals eventually decay exponentially until the slope is affected by the background. The two signals are shifted relative to each other to emphasize the common exponential decay constant. For sufficiently fast ramps (heating rate higher than 10 K/s) the exponential decay constant depends only on the species and the outgassing temperature, but is independent of the loading temperature (which determines the amount of hydrogen) as well as from the ramp velocity (e.g. 15 and 20 K/s). For the holding temperature of 2000 K the exponential decay of the deuterium signal is fitted using a nonlinear least-squares fit. The derived decay for the single crystalline sample and the poly crystalline specimen is identical within the measurement accuracy. Generally, for the data used in the present paper we do not see a difference in the steady-state decay constants between single and poly crystalline samples. This largely excludes a potential influence from different trap concentrations or grain boundaries [17].

Figure 6 shows a series of deuterium degassing signals for the single crystal: the plateau temperature is the same, 2200 K. The ramps are 15 or 20 K/s (the leftmost signal results from

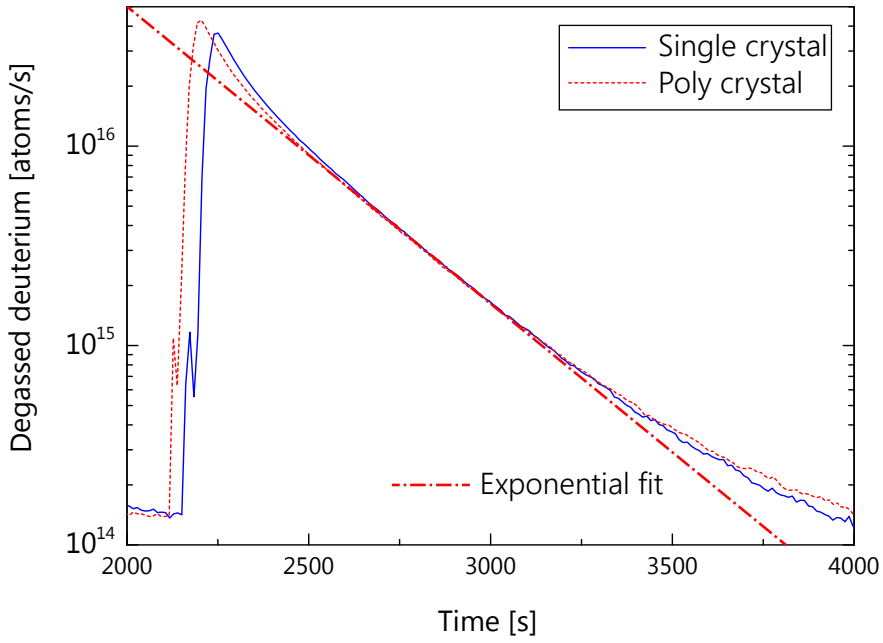

Figure 5: Thermal desorption spectra of the single and the poly crystal. The gas loading conditions are equal: 2000 K for 30 min in 500 mbar deuterium atmosphere. The degassing conditions are also the same, a 20 K/s ramp up to a 2000 K plateau. The spectrum of the single crystal is shifted to the left to match the exponential decay of the poly crystal - although at the beginning of the ramp the deuterium atom degassing signals differ, both samples can be fitted with the same exponential fit parameters after the temperature has reached the plateau and the hydrogen concentrations in the samples follow the fundamental mode ($m = 1$) profile.

a 15 K/s ramp, the other two measurements are performed with 20 K/s ramps). In addition the loading conditions varied; the leftmost signal is from a sample loaded at 2200 K, the signal in the middle from a sample loaded at 2000 K and the rightmost at 1800 K. It can be seen that the total amount of deuterium increases with increasing gas loading temperature. Nevertheless the decay constant of the signal at later times (here between t=2500 s and t=2900 s) for the three loading conditions is identical. Please note that for clarity and ease of comparison both, in figure 5 and 6 all TDS spectra have been shifted horizontally (along the time-axis) such that for spectra measured with the same peak temperature the spectra are aligned with respect to the effusion flux of $f = 2 \times 10^{15}\,\mathrm{D/s}$, which is sufficiently large to be not affected by the background level of $f_0 = 3 \times 10^{14}\,\mathrm{D/s}$. At the later stages of the outgassing this background level becomes apparent in the reduction of the signal decay rate. The TDS-spectra exhibit initially a faster signal decay once the temperatures have reached their plateau values compared to the single-exponential decay later on. This is due to the presence of higher order terms $(n > 0, m > 1)$ contributing to the concentration profile. However, these contributions decay faster with time than the fundamental mode $(m = 1)$, cf. Eqs. 2 and 3 and do not affect the decay later on. The estimated decay rates $\gamma(T)$ for protium and deuterium

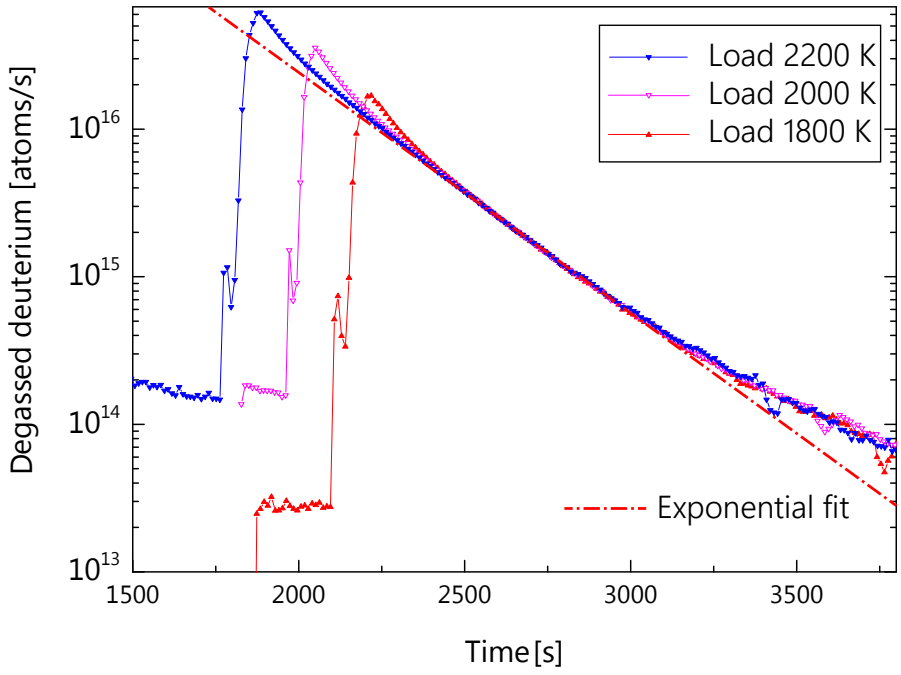

Figure 6: Thermal desorption spectra for deuterium gas loaded single crystalline sample. The spectra show three different sample loading temperatures (from left to right: 2200 K, 2000 K, 1800 K) with a temperature profile $T(t)$ of the desorption cycle: A temperature ramp of 15 (the leftmost spectrum) or 20 K/s up to 2200 K, then keeping the sample at this temperature plateau until the signal approaches the background level (spectra have been horizontally shifted for clarity). For all plateau temperatures the exponential decay of the deuterium signal is fitted using a nonlinear least-squares fit.

are displayed in figure 7a as function of the inverse outgassing temperature. Both data sets have been fitted independently with an exponential $\gamma(x) = A\exp(E \cdot x)$ with $x = 1/\mathrm{kT}$. For the case of protium this yields as maximum-likelihood estimate $\mathrm{A_H} = 0.0212 \cdot 1/\mathrm{s}$ and an activation energy for the diffusion of $\mathrm{E_A^H} = 0.28\,\mathrm{eV}$. For the case of deuterium this yields as maximum-likelihood estimate $\mathrm{A_D} = 0.0167 \cdot 1/\mathrm{s}$ and the same activation energy for the diffusion of $\mathrm{E_A^D} = 0.28\,\mathrm{eV}$. Based on Eqs. 7 and 8 the pre-exponential factor $\mathrm{D_0^H}$ of Eq. 8 can be obtained via

$$\mathrm{D_0^H} = \left(\frac{a}{\xi_1}\right)^2 \mathrm{A_H} \tag{10}$$

and analogously for deuterium.

The standard parameter uncertainties provided by maximum-likelihood estimation schemes like Levenberg-Marquardt are derived from (the inverse of) the local Hessian matrix at the optimum [18]. It is known that these uncertainties may be misleading if the model is not linear in its parameters [19, 20] as it is the case here. To ensure a realistic assessment of the uncertainties a Bayesian approach is applied [21]: Using a uniform prior probability distribution for the parameters 1000 posterior samples $\{\mathrm{D_0}, \mathrm{E_A}\}_i, i = 1, \ldots, 1000$ are sampled

from the posterior distributions $p(\mathrm{D}_0, \mathrm{E}_\mathrm{A} \mid \mathbf{d})$ using rejection sampling for both, protium and deuterium. The obtained samples are given in figure 7b. In addition the maximum-likelihood parameters from figure 7a are indicated by crosses. Based on the marginal densities of the activation energies $p(\mathrm{E}_\mathrm{A} \mid \mathbf{d})$ which are shown at the bottom of figure 7b an uncertainty of 0.06 eV for the diffusion activation energies is derived. It should be pointed out that the probability distributions are asymmetric around the mean-value and thus are not Gaussian distributions. For comparison also the parameter values of Frauenfelder for protium($\mathrm{E}_\mathrm{A}^\mathrm{H} = 0.39\,\mathrm{eV}$ and $\mathrm{D}_0^\mathrm{H} = 4.1 \cdot 10^{-3}\mathrm{cm}^2/\mathrm{s}$) is given.

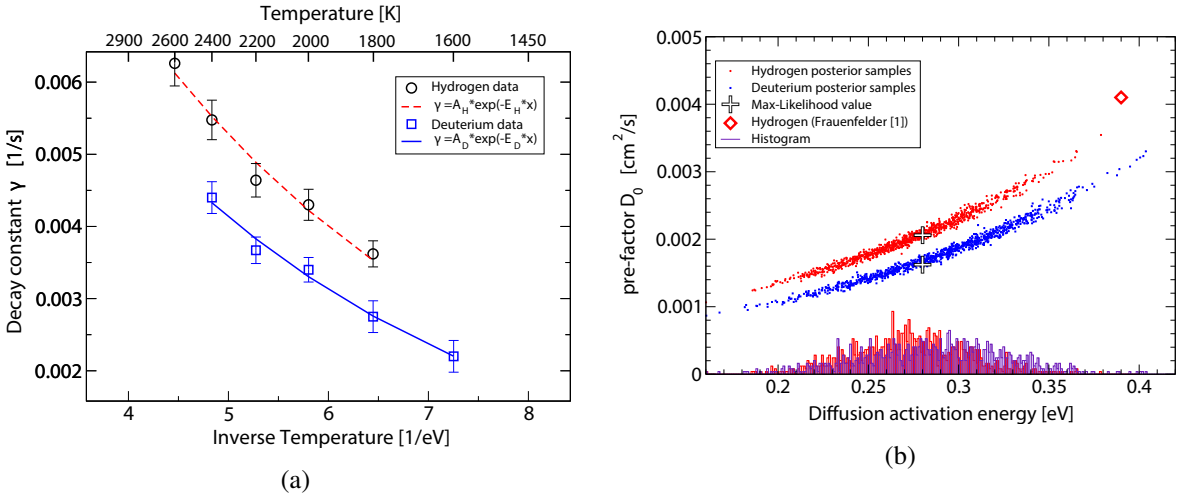

(a) (b)

Figure 7: Left panel: The decay constants for different holding temperatures are plotted versus the inverse of the holding temperature. The decay constants for deuterium and protium are fitted independently to equation 7, resulting in both cases in a diffusion activation energy of $E_A = 0.28\,\mathrm{eV}$. The pre-factors of the exponential fit are $A_H = 0.0212 \cdot 1/\mathrm{s}$ and $A_D = 0.0167 \cdot 1/\mathrm{s}$ for hydrogen and deuterium, respectively. Right panel: Samples of the posterior probability distributions $p(\mathrm{E}_\mathrm{A}, \mathrm{D}_0 \mid \mathbf{d})$ for protium and deuterium. Also indicated is the corresponding value of Frauenfelder for hydrogen [1] and the most likely values. At the bottom of the panel the (non-normalised) marginal distributions $p(\mathrm{E}_\mathrm{A} \mid \mathbf{d})$ for protium and deuterium are displayed.

7. Conclusion and Outlook

A combined experiment and modeling approach is used to determine the diffusion and solubility parameters of protium and deuterium in poly and single crystalline tungsten. The derived results for the diffusivity constant differ considerably from the commonly used and recommended values. Instead of $E_A = 0.39\,\mathrm{eV}$ for the activation energy we obtain $E_A = 0.28 \pm 0.06\,\mathrm{eV}$ for both, protium and deuterium. The prefactors are $\mathrm{D}_0^\mathrm{H} = 2.06 \cdot 10^{-3}\mathrm{cm}^2/\mathrm{s}$ and $\mathrm{D}_0^\mathrm{D} = 1.60 \cdot 10^{-3}\mathrm{cm}^2/\mathrm{s}$, respectively. Based on our results the suspicion that Frauenfelder's values for the diffusion coefficient are distorted by data from outgassing temperatures below 1400 K and hence also non-solute diffusion effects came into play appears reasonable [6, 9].

The ratio $q_{exp} = A_D/A_H = 1.27$ is not too far off from $q_{th} = \sqrt{2}/1 = 1.41$, which is predicted by harmonic theory. However, simultaneous fits of protium and deuterium measurements with the same activation energy and employing q_{th} do not yield satisfying results. It should be pointed out that deviations from the classical mass scaling have also been observed for other metal-hydrogen systems [22].

The measurements are presently still ongoing: Besides the deviation from the classical scaling one of the issues presently being scrutinized is the origin of the reproducible spike during the initial phase of the heating ramps (see eg. at t = 2200 in figure 5). Measurements with hollow tungsten cylinders of twice the surface but of significantly lower mass have shown that the first increase can to some extend be attributed to the release of atoms adsorbed on the surface of the sample and of the glass tube walls. However, comparisons of the whole loading-degassing cycle data with the 3-D TDS-simulations still indicate a slightly delayed rise of the hydrogen emission after the spike up to a temperature of approximately 1500 K. An assignment to intrinsic trapping does not appear convincing because single and poly crystalline specimen yield identical results. At present the formation of a thin tungsten-oxide layer at the surface during the cooldown phase and subsequent evaporation during the temperature rise [16] is considered to be the most likely explanation and under ongoing investigation. For that a larger tungsten cylinder is used: the increased volume-to-surface ratio should not only help to disentangle volume and surface effects but will also improve the signal-to-noise ratio of the outgassing process further.

References

[1] Frauenfelder R 1969 *J. Vac. Sci. Technol.* **6** 388

[2] Wright G, Mayer M, Ertl K, de Saint-Aubin G and Rapp J 2011 *J. Nucl. Mater.* **415** S636–S640

[3] Schmid K, von Toussaint U and Schwarz-Selinger T 2014 *J. Appl. Phys.* **116** 134901

[4] Hodille E, Bernard E, Markelj S, Mougenot J, Becquart C, Bisson R and Grisolia C 2017 *Physica Scripta* **T170** 014033

[5] Causey R 2002 *J. Nuclear Materials* **300** 91–117

[6] Heinola K and Ahlgren T 2010 *Journal of Applied Physics* **107** 113531

[7] Ahlgren T and Bukonte L 2016 *J. Nucl. Materials* **479** 195–201

[8] Johnson D and Carter E 2010 *J. Mater. Res.* **25** 315–327

[9] Fernandez N, Ferro Y and Kato D 2015 *Acta Materialia* **94** 307–318 ISSN 1359-6454

[10] De Vos J C 1954 *Physica* **20** 690–714 ISSN 0031-8914

[11] Salançon E, Dürbeck T, Schwarz-Selinger T, Genoese F and Jacob W 2008 *J. Nucl. Mater.* **376** 160–168

[12] Allen R D, Glasier L F and Jordan P L 1960 *Journal of Applied Physics* **31** 1382–1387

[13] Hust J and Lankford A 1984 Thermal conductivity of aluminum, copper, iron and tungsten from temperatures from 1 K to the melting point NBSIR 84-3007 National Bureau of Standards, U.S. Department of Commerce

[14] Carslaw H and Jaeger J 2011 *Conduction of Heat in Solids* 2nd ed (Oxford: Oxford Science Publications)

[15] Rasch K D, Siegel R W and Schultz H 1980 *Philosophical Magazine A* **41** 91–117

[16] Lassner E and Schubert W D 1998 *Tungsten: properties, chemistry, technology of the element, alloys, and chemical compounds* 1st ed (New York: Springer Science)

[17] Oda T 2016 *Fusion Engineering and Design* **112** 102–116

[18] Press W, Teukolsky S, Vetterling W and Flannery B 2007 *Numerical Recipes* 3rd ed (Cambridge: Cambridge University Press)

[19] Sivia D S 2006 *Data analysis—a Bayesian tutorial* 2nd ed (Oxford: Clarendon Press)

[20] W von der Linden V D and von Toussaint U 2014 *Bayesian Probability Theory* 1st ed (Cambridge: Cambridge University Press)

[21] von Toussaint U 2011 *Review of Modern Physics* **11** 943–999

[22] Alefeld G and Völkl J 1978 *Hydrogen in Metals I* (Berlin: Springer)